Xe_n clusters in the alpha cages of zeolite K*A*

Cynthia J. Jameson
Department of Chemistry M/C-111, University of Illinois at Chicago, Chicago, Illinois 60607

A. Keith Jameson
Department of Chemistry, Loyola University, Chicago, Illinois 60626

Rex E. Gerald II[a] and Hyung-Mi Lim
Department of Chemistry M/C-111, University of Illinois at Chicago, Chicago, Illinois 60607

(Received 26 June 1995; accepted 22 August 1995)

We have observed the individual signals of the Xe_n clusters ($n=1-5$) trapped in the alpha cages of zeolite K*A*. The ^{129}Xe NMR chemical shift of each cluster in zeolite K*A* is larger than that of the corresponding Xe_n cluster in zeolite Na*A*. The temperature dependence of the chemical shifts of the clusters vary systematically with cluster size as they do in Na*A*, but the change of the temperature coefficients with n is somewhat more pronounced for Xe_n in the cages of K*A* than in Na*A*. The Xe_n chemical shifts and their variation with temperature are reproduced by the grand canonical Monte Carlo (GCMC) simulations. GCMC simulations of the distribution of the Xe atoms among the alpha cages in K*A* provide the fractions of cages containing n Xe atoms which agree reasonably well with the observed equilibrium distributions. The characteristics of Xe distribution and chemical shifts in K*A* are compared with that in Na*A*. © *1995 American Institute of Physics.*

I. INTRODUCTION

^{129}Xe NMR is widely used in the characterization of microporous materials. In zeolites,[1–4] polymers,[5–7] coals,[8] clays,[9] and other porous materials,[10,11] or even agglomerated microspheres,[12] the mobility of the Xe atoms is such that only one Xe signal is usually observed in the NMR spectrum. The average chemical shift of the single peak under fast exchange and its dependence on the temperature and the average Xe occupancy are all that can be observed in nearly all microporous solids. In these cases the Xe chemical shift is known empirically to depend on zeolite pore and channel dimensions,[13–16] location of cations,[17] coadsorbed molecules,[18,19] dispersed metal atoms[3,4,20–26] and paramagnetic ions,[27,28] on water content,[29,30] blockage of pores by coking,[31,32] domains of different composition or crystallinity,[33] etc. The relationship of the ^{129}Xe chemical shift to cavity size and shape, average xenon loading, temperature, and type of cations is still not completely understood. If we can understand these quantitatively, we should be able to make a clearer connection between the average chemical shift of the Xe signal under fast exchange with parameters of the zeolite structure, although it may not be possible to predict the structure just from the average chemical shift. In particular it is possible to use computer simulations at the grand canonical level to model the average chemical shift of the single peak under fast exchange and its dependence on the temperature and the average occupancy. Such simulations in turn can provide details of distributions and dynamics of the sorbate atoms. Varying the parameters of the simulations in order to reproduce the observed quantities could, in principle, lead to an optimum description of the system. However, this is usually not a rigorous way to proceed with such highly averaged observables because there are usually far more model parameters that can be varied than there are measured quantities. Instead we choose to carry out systematic studies in (a) specifically those zeolites (type *A*) of known structure where the position of every Si and Al atom and also every charge-balancing cation is known; (b) where the actual equilibrium distribution of cages containing specifically known numbers of Xe atoms is directly observed; (c) where the average chemical shift of ^{129}Xe in cages containing a specific number of Xe atoms is individually observable, as well as its temperature dependence; (d) where the temperature dependence of the average Xe occupancy (the adsorption isotherm) can also be observed at the same time. In such a system, for example, Xe in Na*A*, we expect to be able to find direct tests of those details of computer simulations that are usually averaged over. This way we would have more critical and detailed constraints on the computer modeling.

We have already seen, by the comparison between the ^{129}Xe NMR spectra of Xe sorbed in Na*A* and in Ca*A*, that the average chemical shift under fast Xe exchange (in the relatively open Ca*A* system) contains in it the information about the individual shifts associated with specific numbers of Xe atoms per cage (or Xe_n clusters), convoluted with the fractions of such cages in the zeolite appropriate to the average occupancy at a given temperature.[34,35] The average chemical shift of the single Xe NMR signal (in Ca*A*) changes as the average occupancy varies with temperature and as the chemical shifts of the Xe_n clusters vary with temperature. In contrast, the individual Xe_n clusters are observed directly in Na*A*; their distributions and their individual chemical shifts have been measured as a function of temperature and loading.[34,36–38] Furthermore, these observed distributions (fractions of alpha cages containing specifically n Xe atoms) and Xe_n individual chemical shifts, and their temperature dependences in Na*A* have been reproduced by a grand canonical Monte Carlo (GCMC) simulation.[39] Therefore it is possible to understand qualitatively how the average

[a]Currently at Argonne National Laboratory.

chemical shift under fast exchange in the open pores of zeolite Ca*A* is determined by the individual properties of cages filled with n Xe atoms. A quantitative interpretation would require that we know in what way the Xe chemical shift is affected by Ca^{2+} ions as opposed to Na^{+}ions in the large cavities of the zeolite. Knowing this would in turn provide us with a better understanding of the dependence of the average Xe chemical shift on the types (and locations) of cations in the zeolite. We could not obtain this information from solely the data for Xe in Ca*A*, however, because of the nature of the averaging that occurs in Ca*A*, throughout the zeolite crystallite rather than just within a single alpha cage.

II. ^{129}Xe CHEMICAL SHIFTS IN CATION-EXCHANGED ZEOLITES

^{129}Xe has been used widely as a means of monitoring exchange of cations in a zeolite and characterizing cation-exchanged zeolites.[17,27,28,41,42] For example, a series of very carefully executed experiments have established quantitatively the changes in the ^{129}Xe chemical shift $\delta(^{129}\mathrm{Xe})$ of xenon in the limit of zero Xe loading, $\lim_{\langle n\rangle_{\mathrm{Xe}}\to 0}\delta(^{129}\mathrm{Xe})$, as Na^{+}ions are exchanged with K^{+}, Rb^{+}, Cs^{+}, Mg^{2+}, Ca^{2+}, Sr^{2+}, Ba^{2+}, Zn^{2+}, Co^{2+}, Ni^{2+}, Cu^{2+}, etc., in zeolite Na*Y*,[27,28] and as Ca^{2+} ions are exchanged with Na^{+} ions in Na*A*.[41] These papers also reported well-documented quantitative changes upon cation exchange in the slopes, $d\delta(^{129}\mathrm{Xe})/d\langle n\rangle_{\mathrm{Xe}}$, of the ^{129}Xe chemical shifts as a function of average Xe occupancy $\langle n\rangle_{\mathrm{Xe}}$. We believe that several factors contribute to these observed changes. The effect of exchanging the cation on the average chemical shift of Xe under fast exchange in a zeolite has to do, in part, with a change in the excluded volume (a larger cation leaves a smaller effective volume over which the Xe–Xe interactions can operate). Another part has to do with the generally larger polarizability of the larger cation, leading to a deeper well in the potential function between the Xe and the cation, thereby altering the one-body distribution of the Xe in the cage. Both of these factors affect the nature of the averaging over the various positions of the Xe atom within the zeolite and thus lead to a change in the average ^{129}Xe NMR chemical shift. Finally, a part of the observed changes has to do with the differences between the ^{129}Xe shielding function itself for a Xe atom interacting with a Na^{+} ion as opposed to a Xe atom interacting with a Cs^{+} ion, for example. Excluded volume alone without a change in either the shielding function or the well-depth in V(Xe–M) would lead to smaller intercepts, $\lim_{\langle n\rangle_{\mathrm{Xe}}\to 0}\delta(^{129}\mathrm{Xe})$, with increasing cation size. The larger the excluded volume for the single Xe in the cage, the smaller will be the contributions to the chemical shift from the oxygens in the immediate vicinity of each cation. Since this is opposite to the trends observed experimentally, the greater well depth associated with V(Xe–M) as the size of the cation M increases must also play a role, and the differences between the unknown shielding functions $\sigma(r_{\mathrm{Xe-M}})$ may themselves contribute to the change in intercept. Excluded volume effects alone would lead to greater slopes, $d\delta(^{129}\mathrm{Xe})/d\langle n\rangle_{\mathrm{Xe}}$, with increasing cation size because the known intermolecular shielding function $\sigma(r_{\mathrm{Xe-Xe}})$ is steeply changing at short distances,[43] and with a larger excluded volume for the xenon atoms, average Xe–Xe distances within the cage become shorter. Therefore, qualitatively, we propose that the observed increase in intercepts, $\lim_{\langle n\rangle_{\mathrm{Xe}}\to 0}\delta(^{129}\mathrm{Xe})$, with increasing ion size (that is, with increasing fraction of larger ion substitution or with increasing ion size at the same fractional substitution) can be attributed to the change in the shielding function $\sigma(r_{\mathrm{Xe-M}})$, and further enhanced by an increase in the well depth of V(Xe–M). On the other hand, to explain the observed slight increase in slope, $d\delta(^{129}\mathrm{Xe})/d\langle n\rangle_{\mathrm{Xe}}$, the increase in excluded volume due to the increase in r_0(Xe–M) with increasing ion size would be sufficient without invoking a change in the shielding function. Although these experiments on Xe in the cation-exchanged faujasites were very carefully done and the results are quantitative, and although they appear to be internally consistent and generally not inconsistent with other known information about Xe adsorption in zeolites, this interpretation is so far only qualitative. There is no clear separation of these various factors which are operating at the same time, resulting in a single average ^{129}Xe chemical shift under fast exchange. Although the extent of cation replacement can be measured by chemical analytical procedures, there is no independent way of finding out whether one-on-one replacement takes place (the replacement cation goes to the same site that the previous cation left), or whether the new cations end up in different types of sites than the ones that had been vacated. It is not unequivocally known that univalent cations occupy identical sites from one cation to another in the faujasites (zeolite *Y* and *X*); thus, a part of the observed change is likely due to larger ions having to take sites which exclude volume in the large cages to which the Xe atoms have access. Furthermore, even when one-on-one replacement does occur, partial cation exchange leads to a statistical distribution of the replacement ions among the sites of the same type, leading to a disordered crystal structure. Since the ^{129}Xe chemical shift is completely averaged over the distribution of such environments, the quantitative interpretation of these comprehensive experimental data is not yet within reach.

How then can we obtain more detailed information than is available from these already very careful systematic experiments on the effects of cation exchange in zeolites? In the same way that the observation of the individual Xe_n clusters in Na*A* provided more detailed information about the distribution of atoms in zeolite cavities and the average chemical shifts for different numbers of Xe atoms in a cavity than was possible from the ^{129}Xe NMR studies of zeolites under fast exchange, the study of Xe_n clusters in various ion-exchanged *A*-type zeolites should provide the fine details that are required to sort out the various factors affecting Xe chemical shifts in ion-exchanged zeolites in general. For example, we already have presented some preliminary conclusions based on the ^{129}Xe NMR signals observed under magic angle spinning (MAS) of Xe_n in zeolite Na*A* that had been dehydrated subsequent to very low levels of Ca exchange.[44]

In this paper we obtain direct information regarding the effect of the cation on the Xe chemical shift in a system where we obtain the same detailed information as was avail-

able in Na*A* (fractions of alpha cages containing n Xe atoms, ^{129}Xe chemical shifts in individual Xe_n clusters, and temperature dependence of the ^{129}Xe chemical shifts in individual Xe_n clusters). We have reported for the first time the observation of the individual peaks corresponding to the Xe_n clusters trapped in zeolite K*A*.[45] Here we provide the ^{129}Xe chemical shifts of the individual Xe_n clusters ($n=1$–5), the temperature dependence of these chemical shifts, and the equilibrium distributions of Xe atoms among the cavities of the zeolite at 573 K, that is, the fractions of the alpha cages which have specifically n Xe atoms. We also report GCMC simulations of Xe in K*A* compared to Xe in Na*A*, which provide detailed information about the effects of the size of the cation on the Xe one-body distribution function, the effects of the size of the cation on the ^{129}Xe chemical shift of the single Xe in an alpha cage, and the separate effects of the larger excluded volume in the cages of zeolite K*A*. The latter are reflected in the changes in the Xe–Xe pair distribution functions, the changes in the Xe_n chemical shifts, and the changes in the Xe_n–Xe_{n-1} incremental shifts in going from Na*A* to K*A*.

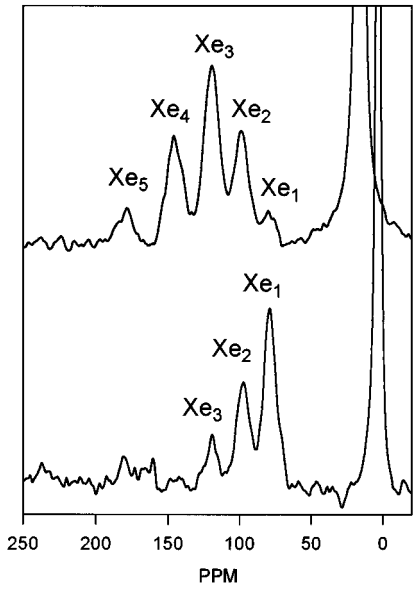

FIG. 1. The ^{129}Xe spectra of xenon occluded in zeolite K*A* recorded at 300 K in samples corresponding to average occupancies $\langle n\rangle_{Xe}=0.78$ (bottom) and 2.54 (top) atoms per cage. The samples are equilibrated at 573 K in an oven for two days and left at 300 K for several months prior to recording the spectrum.

III. EXPERIMENTAL AND THEORETICAL METHODS

A. Sample preparation and ^{129}Xe NMR spectroscopy

The samples of Xe in zeolite K*A* were prepared in exactly the same way as the Xe in Na*A* samples, as described earlier.[34] A measured mass of dry zeolite (Linde 3A) is placed in a calibrated sample tube of about 0.2–0.25 m*l*. It is then dried to remove any last traces of moisture (~370 °C, 16 h, thin-bed conditions). A known number of moles of xenon (99.9% ^{129}Xe) is sealed into the sample tube with dry zeolite in place. The sample tube is then heat-treated as follows. The mobility of the xenon atoms in zeolite K*A* is exceedingly slow. Initially, the only evidence for occluded xenon was a net decrease of about 5 ppm in the chemical shift of the free gas peak in a sample which was ramped down in temperature from 750 to 550 K over a period of 5 months. The mobility appears to be quite slow below 550 K and sample equilibration (that is, the achievement of the equilibrium distribution of the Xe atoms among the alpha cages and with the bulk gas outside the crystallites) may not be possible in a reasonable length of time at temperatures close to room temperature. In addition, the characteristic time constants for the relaxation of ^{129}Xe nuclear spins are substantially longer in K*A* than in Na*A*. Figure 1 shows ^{129}Xe NMR spectra recorded at 300 K of xenon occluded in K*A* after equilibration for several hours at 573 K and then at room temperature for several months.

A pulse width of $\pi/4$ with a relaxation delay of 30 s was found to give relative peak intensities indistinguishable from longer delay times. Spectra were taken on both Varian VXR-300 (at 300 K) and Bruker AM-400 (variable temperature) spectrometers. The number of transients acquired was typically 2000–6000. Temperatures were measured using the known CH_n–OH temperature-dependent ^{1}H chemical shift in methanol (below 300 K) or in ethylene glycol (above 280 K) and could be controlled to within about 0.2 K. Spectra were taken with the spectrometer unlocked, B_0 set to a predetermined resonance frequency at 300 K for the methylene proton of ethylene glycol, and then the temperature changed as desired. Measurements at other temperatures are carried out at exactly the same field. This is done as follows: We had previously found that the resonance frequency of ^{13}C in methane at low density is virtually temperature independent and provides us with a convenient reference for setting B_0 reproducibly back to the same value each time. At each temperature, the magnetic field is adjusted so that the ^{13}C resonance frequency is 100.613 805 MHz exactly and the ^{1}H resonance frequency was measured in ethylene glycol (or methanol). These ^{1}H (CH_n) frequencies are used to set the magnetic field back to the same constant value for all ^{129}Xe measurements at any temperature.

B. Grand canonical Monte Carlo simulations

The simulation box is a unit cell of dehydrated zeolite K*A*, $\{K_{12}[(AlO_2)_{12}(SiO_2)_{12}]\}_8$, $a=24.6000$ Å, with the Si, Al, O, and K positions according to the single-crystal x-ray refinement by Pluth and Smith.[46] Each unit cell contains eight large cavities (alpha cages) and eight small ones (beta cages). The oxygen atoms bridging the Si and Al atoms form rings with four, six, and eight oxygens. In the pseudo-unit cell, 8 of the 12 K atoms occupy positions in the 8 six-rings (nominally site I). While the Na atom is small enough to lie near the center of a six-ring, the K atom is considerably displaced with 1.5 atoms pointing into the sodalite unit and 6.5 atoms into the alpha cage. Also, almost one atom lies opposite a four-ring (nominally site III) of which some fraction projects from the four-ring into the sodalite unit and the remainder into the alpha cage. A systematic arrangement of the ions in the unit cell simulation box leads to lower energy, just as in

zeolite Na*A*. The sites are analogous to the Na sites as known from x-ray refinement. The only difference between what we have designated as the primed and unprimed sites is that the primed sites are displaced more into the sodalite cage whereas the unprimed sites are displaced more into the alpha cage. The cation sites of Na*A* and K*A* are related as follows:

$$64\mathrm{Na(I)} \rightarrow 52\ \mathrm{K(I)} + 12\ \mathrm{K(I')},$$

$$24\mathrm{Na(II)} \rightarrow 24\ \mathrm{K(II)},\ \mathrm{K\ centered\ in\ each\ 8\text{-}ring\ window},$$

$$8\mathrm{Na(III)} \rightarrow 4\ \mathrm{K(III)} + 4\ \mathrm{K(III')}.$$

We could choose to average the primed and the unprimed positions with respect to in/out positions in the alpha cage. However, this makes the energy of the zeolite much higher because the in/out arrangement of the large K^+ ions is precisely the way by which the zeolite minimizes its energy.[46] Furthermore such an average would not give a realistic alpha cage size for the Xe atoms. Therefore this would be a poor choice if we want ^{129}Xe chemical shifts and/or fractional occupancies P_n. We therefore made a choice of K atom positions to reflect the relative occupancies of the I and I′ and of III and III′ sites indicated by the x-ray work. We choose the in/out arrangement with respect to the sodalite cage such as to have half of the sodalite cages have 2K(I′) and the other half have K(I′)+K(III′). We placed K(III) and K(III′) in the same way as we put Na(III) into the simulation box for Na*A*, except that for K*A* we alternated K(III′) and K(III). The sodalite cages with K(III′) have only one K(I′); the other sodalite cages [next to K(III)] have 2K(I′) and the primed ions are sited in 6-rings which are farthest apart from each other. This distribution of ions leads to only two types of alpha cages within the unit cell simulation box and yet reflects the actually observed partial occupancies of K^+ sites found in x-ray diffraction. With this simulation box we expect to have reasonably realistic alpha cage internal volumes accessible to the Xe atoms which can provide reasonably realistic averages of P_n and ^{129}Xe chemical shifts. The zeolite is assumed to be rigid in the simulations, although there is theoretical evidence that low-frequency window fluctuations should be accessible at room temperature.[47]

The GCMC method is implemented in the same way as described previously.[39] The V(Xe–Xe) potential is a Maitland–Smith functional form fitted to the best Xe–Xe potential for the pair interaction, as was used for Xe in Na*A*,

$$U(r) = \epsilon\left\{\frac{6}{n-6}\,\bar{r}^{-n} - \frac{n}{n-6}\,\bar{r}^{-6}\right\}, \quad \bar{r} = r/r_{\min},$$

where n is allowed to vary with $\bar{r}$ according to $n = 13 + 11(\bar{r}-1)$. The effective V(Xe–O) potential used in the simulation is a Lennard-Jones form with the same r_0 and ϵ/k parameters as was used for Xe in zeolite Na*A*. In other words, we assume that the pairwise interaction of the Xe atom with the atoms of the framework is the same for zeolite K*A* as for Na*A*. There is not too much known about the parameters for the Lennard-Jones potential describing the pairwise Xe–K interactions in a zeolite. Kiselev and Du suggested $r_0 = 3.7021$ Å and $\epsilon/k = 138.59$ K, based on the Kirkwood–Muller approximation and fitting the adsorption of Xe in zeolite K*X*.[48] Pellenq and Nicholson have derived potential parameters for rare gases in zeolites using a Born–Mayer repulsive term and in-crystal dispersion coefficients and the Tang–Toennies damping function.[49] They concluded that the Kiselev and Du potential functions for Xe in a zeolite have a repulsive part that is too weak, leading to effective channel diameters that are too large. Indeed we had found that using the Kiselev and Du parameters for Na and O for Xe in Na*A* leads to an alpha cage that is effectively too large, which leads to too large a maximum number of Xe atoms that can be observed at the highest loadings at room temperature. As our first attempt, we use a potential that differs from the effective V(Xe–Na) that we used for Xe in zeolite Na*A* in that r_0 is somewhat larger and the well depth ϵ/k is greater for K compared to Na, $r_0 = 3.75$ Å and $\epsilon/k = 90$ K for the Lennard-Jones function V(Xe–K). The zeolite contribution to the ^{129}Xe chemical shift is assumed to be pairwise sums just like the energy sums, except summing over terms from pair shielding functions rather than potential functions. We use a shielding function $\sigma(^{129}\mathrm{Xe},\ \mathrm{Xe}\cdots\mathrm{O_{zeol}})$ and $\sigma(^{129}\mathrm{Xe},\ \mathrm{Xe}\cdots\mathrm{K_{zeol}})$ which has been derived from *ab initio* quantum mechanical calculations of the ^{39}Ar shielding in the presence of fragments of the K*A* lattice, representing 4-, 6-, and 8-rings of the zeolite.[50] The $\sigma(^{129}\mathrm{Xe},\ \mathrm{Xe}\cdots\mathrm{Xe})$ shielding function is the same as was used in the Na*A* simulation.[39] The potential functions and the shielding functions are all cut-and-shifted in the usual manner.[51] The Norman–Filinov technique is used; a displacement step is followed by two steps of particle creation or annihilation attempts.[52] An attempted move is accepted with a probability P_{acc} given by

$$P_{\mathrm{acc}} = \min[1, \exp(-\Delta E/kT)], \quad \Delta E/kT \leqslant 180,$$

$$P_{\mathrm{acc}} = 0, \quad \Delta E/kT > 180,$$

and ΔE is calculated from the configurational energy change between the old and new configuration and the imposed value of the configurational chemical potential. Some number of 10^5 cycles were discarded prior to the typically one million cycles constituting the simulation proper, for each choice of chemical potential and temperature. All calculations were done on an IBM RISC/6000 model 560 and model 365. Data were collected as described previously[39,40] to yield distributions (fractions of cages having nXe atoms), one-body distribution functions, pair distribution functions, and properties of the individual Xe_n clusters.

IV. RESULTS

It can be estimated that the larger diameter of the K^+ ion compared to the Na^+ ion and the ''in–out'' arrangements of the K^+ ions in the cages of K*A* reduces the cavity volume by nearly the equivalent of 1.5 Xe atoms (based on the ionic radii). The largest Xe_n cluster observed by us in Na*A* is Xe_8.[34] Thus, the largest Xe_n cluster that might be expected in an alpha cage of zeolite K*A* is Xe_6. The larger diameter of the K^+ ion compared to the Na^+ ion and its location at the center of each of the 8-ring windows of the K*A* alpha cage,[46] in contrast to the off-center location of Na^+ in the 8-ring

TABLE I. Xe chemical shifts, ppm, and Xe_n clusters in zeolite K*A*, recorded at 300 K, compared with Na*A*.

n		1	2	3	4	5	6	7	8
K*A*	$\delta(Xe_n)$	79.5	98.4	119.7	145.4	180.5			
	$\delta(Xe_n)-\delta(Xe_{n-1})$		18.9	21.3	25.7	35.1			
Na*A*	$\delta(Xe_n)$	74.8	92.3	111.7	133.2	158.4	183.5	228.3	272.3
	$\delta(Xe_n)-\delta(Xe_{n-1})$		17.5	19.4	21.5	25.2	25.1	44.8	44.0
K*A*–Na*A*	$\delta(Xe_n)_{KA}-\delta(Xe_n)_{NaA}$	4.7	6.1	8	12.2	22.1			

windows of Na*A*,[53] reduce the rate of cage-to-cage and bulk-to-cage migration of Xe atoms in K*A* substantially, in comparison to the measured rates in Na*A*.[54] The much broader ^{129}Xe spectra of the Xe_n under magic angle spinning in K*A* (Ref. 55) compared to Xe in Na*A* (Ref. 44) suggests that there is cation disorder in our sample of K*A*. From the x-ray diffraction data it is known that the K*A* unit cell has a larger number of nonequivalent types of cation sites and since each of these are only partially populated, K*A* has more cation disorder than Na*A*.[46]

The typical ^{129}Xe NMR spectra are shown in Fig. 1. Just as for the Xe_n clusters in the alpha cages of Na*A*, the spectra in Fig. 1 have identical peak positions in all samples when the spectra are taken at the same temperature. The intensities reflect the equilibrium distribution of Xe atoms among the alpha cages of zeolite K*A* at 573 K. The chemical shift of the peaks assigned to clusters Xe_1 through Xe_5 and the incremental shifts from one cluster to the next are listed in Table I. Several trends are immediately apparent. The chemical shift of each Xe_n cluster relative to the free Xe atom is larger for Xe_n in K*A* than for Xe_n in Na*A*: 4.7, 6.1, 8.0, 12.2, 22.1 ppm larger in K*A* than Na*A* for Xe_1, Xe_2, Xe_3, Xe_4, and Xe_5, respectively. Furthermore, the increments in the ^{129}Xe chemical shift of adjacent cluster peaks are somewhat larger than those found in zeolite Na*A*, 18.9, 21.3, 25.7, 35.1 ppm in K*A* vs 17.5, 19.4, 21.5, 25.2 ppm in Na*A*. These are very interesting differences which we hoped to be able to understand with the help of GCMC simulations.

The observed temperature dependences of the average ^{129}Xe chemical shift of the Xe_1, Xe_2, Xe_3, and Xe_4 clusters in the alpha cages of K*A* are shown in Fig. 2, where they are compared with the same clusters in Na*A*. The observed temperature dependences of the ^{129}Xe chemical shifts of the Xe_n clusters in the alpha cages of zeolite K*A* follow the same qualitative trends as those for the Xe_n clusters in Na*A*. The chemical shift of the single Xe atom in an alpha cage decreases whereas the chemical shift of the large clusters increases, with increasing temperature. The slope $d\delta(Xe_n)/dT$ is somewhat more pronounced for a single Xe atom in K*A* than in Na*A*, as can be seen in Fig. 2. For Xe_4 in K*A* the temperature coefficient is clearly greater than that for Xe_4 in Na*A*.

The results from the grand canonical Monte Carlo simulations are shown in Figs. 3–5. The fractions of *occupied* alpha cages containing *n* Xe atoms, $g(n)$, are shown in Fig. 3, where they are compared with experimental fractions obtained directly from the intensities of the peaks. Shown here are the distributions obtained from simulations at very nearly the same $\langle n\rangle_{Xe}$ as the experimental values. We find that $g(n)$ for a fixed $\langle n\rangle_{Xe}$ is only slightly dependent on temperature. The simulated distributions at 573 K for the same $\langle n\rangle_{Xe}$ are quite similar to those at 300 K. There are two types of slightly idealized alpha cages in the simulation box. The $\langle n\rangle_{Xe}$ of the two types of cages is slightly different (the difference diminishing with increasing loading), with the alpha cage containing K(III) having the larger occupancy. The greater cation disorder in the crystallites shown by the x-ray diffraction results corresponds to more types of alpha cages than the two used in our simulation box and only the average is observed experimentally. Figures 4 and 5 show the one-body distribution functions for Xe_1 and Xe_6, respectively, for those cages containing K(III). The other type of cage has a quite different one-body distribution. To place the asymmetry of the one-body distribution in context, we note that K(III) is located in the (21,10) voxel at level 10. We also note that the shape of the one-body distribution for Xe_6 is more qualitatively different from Xe_1 in K*A* than is the one-body distribution found for Xe_8 compared to Xe_1 in Na*A*. We note that the one-body distribution for Xe in K*A* is more unsymmetrical than that for Xe in Na*A*. This is due in large part to the two types of K sites in the 6-rings in K*A* in contrast with the single (I) site in Na*A*.

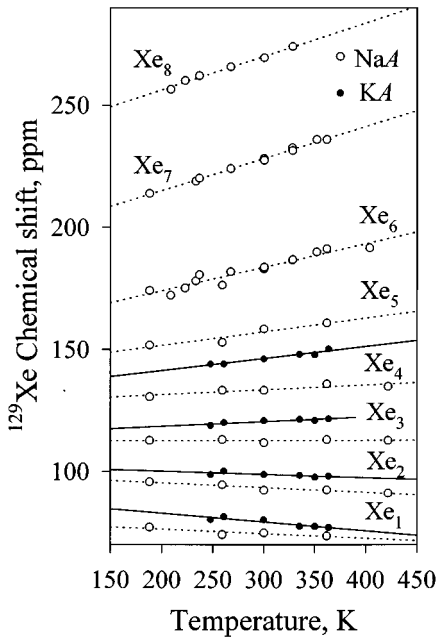

FIG. 2. The observed temperature dependence of the ^{129}Xe chemical shifts of the Xe_n clusters in the alpha cages of zeolite K*A* (●) compared to Xe_n in Na*A* (○).

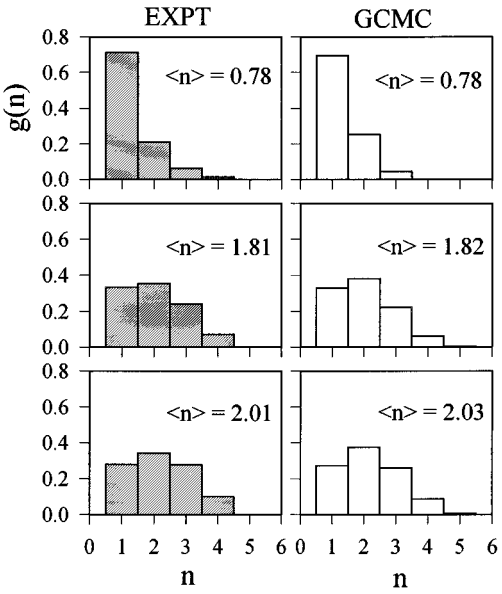

FIG. 3. The distribution of Xe atoms among the alpha cages of zeolite K*A*. Given are the fractions $g(n)$ of the *occupied* alpha cages containing n Xe atoms, from experiments and GCMC simulations.

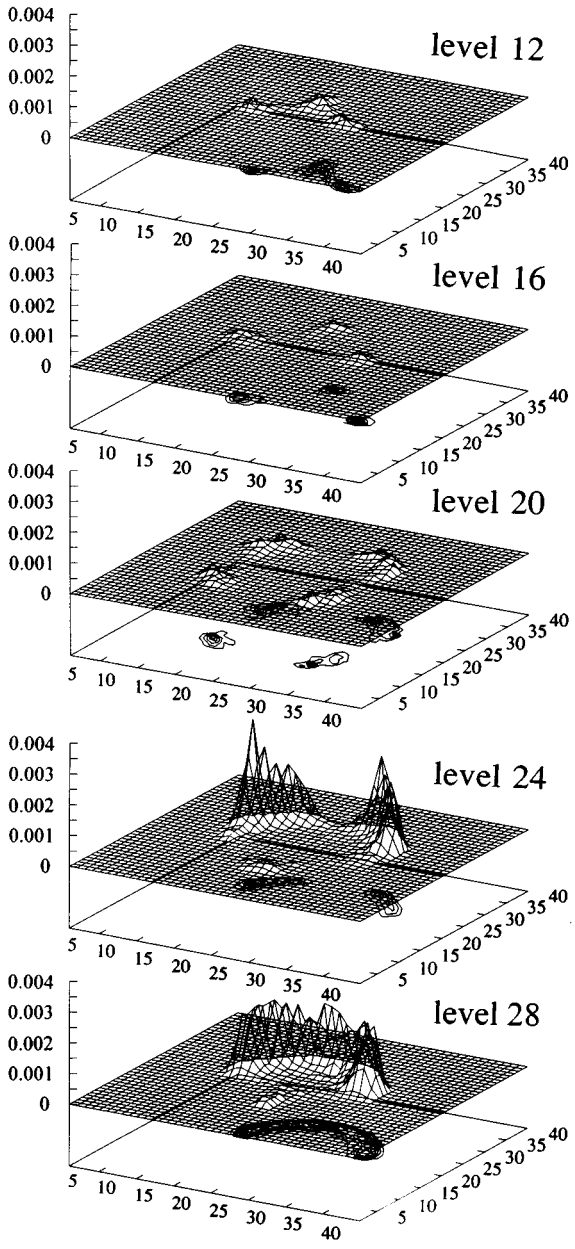

FIG. 4. The one-body distribution function for Xe_1 in an alpha cage of zeolite K*A* at various planes parallel to the 8-ring windows of the alpha cage. The volume-excluding effect of the K ion in site (III) is clearly seen. The center of the K(III) ion is located in the (21,10) voxel at level 10.

Finally we see the GCMC average of the ^{129}Xe chemical shifts for the individual Xe_n clusters in the alpha cages of K*A* in Fig. 6. The shielding functions for Xe–O, Xe–Na, and Xe–K derived from Ref. 50 using scaling procedures described in Ref. 43 were used in the GCMC averaging. The agreement with the previously published temperature dependence for the Xe_n clusters in Na*A* is excellent. These are the first calculated temperature dependence of Xe_n in K*A*. Figure 6 compares directly the results of GCMC simulations with the experimental results. The trends are well reproduced, the slope systematically changing as n increases. Although we only have experimental data for the temperature dependence of Xe_1 to Xe_4 to compare with, we also show the GCMC averages for Xe_5 and Xe_6, which have more pronounced temperature coefficients than the GCMC averages of ^{129}Xe chemical shift in Xe_5 and Xe_6 in Na*A*. In fact the temperature coefficients for Xe_5 and Xe_6 chemical shifts in K*A* are very similar to those for Xe_7 and Xe_8, respectively, in Na*A*.

V. DISCUSSIONS

Without benefit of GCMC simulations we could have predicted qualitatively the trends that are observed. Our original interpretation is that a larger Xe_1 chemical shift is observed in K*A* due to the more pronounced deshielding nature of the ^{129}Xe intermolecular shielding function for Xe–K interactions compared to the Xe–Na shielding function.[50] When coupled with the deeper potential well for Xe–K interactions compared to Xe–Na interactions, this leads to a larger average chemical shift for Xe_1. On the other hand, the somewhat larger r_0 for the Xe–K potential function, coupled with the in–out arrangements of the K ions in the cages, leaves a smaller volume within the cage in which the Xe–Xe contributions are averaged over. When combined with the steeply changing $\sigma(r_{\mathrm{Xe-Xe}})$ shielding function at shorter distances, this leads to larger averages for the individual Xe_n cluster shifts $\delta(Xe_n)$ $(n=2-6)$ in K*A* compared to Na*A*. This, in turn leads to differences $[\delta(Xe_n)_{KA} - \delta(Xe_n)_{NaA}]$ which are uniformly greater than zero. Qualitatively, this is indeed what is observed experimentally.

Based on the GCMC simulations, we show in Tables II and III the partitioning of these chemical shifts into cation contributions, O contributions and Xe–Xe contributions. We see in Table II that in the Xe_n cluster shieldings in Na*A*, contributions from the Xe–O interactions increase as the cages become more crowded, and the Xe–Na contribution increases only slightly. The largest changes come from the Xe–Xe contributions which increase nonlinearly with cluster

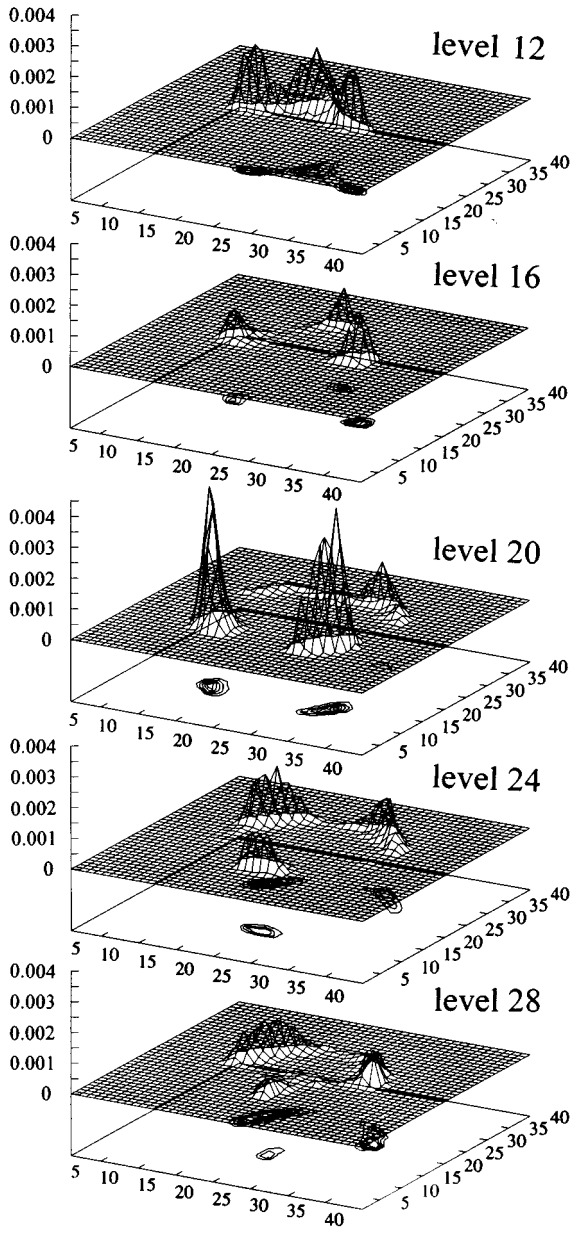

FIG. 5. The one-body distribution function for Xe_6 in an alpha cage of zeolite K*A*. A comparison with Fig. 4 shows that this distribution is more peaked than that for a single Xe but the general features are similar.

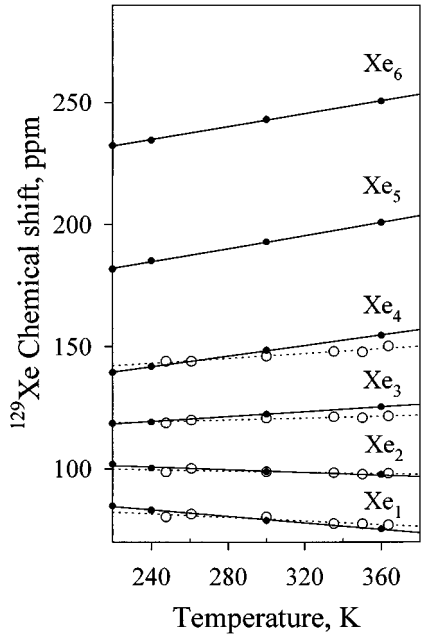

FIG. 6. The results of the GCMC simulations (●) of the temperature dependence of the Xe_n chemical shifts in the alpha cages of zeolite K*A* are compared with those observed experimentally (○).

size as the range of Xe–Xe distances over which the averaging takes place becomes narrower and moves to shorter values. This clearly demonstrates the origin of the much larger increment between Xe_7 and Xe_6 and between Xe_8 and Xe_7 cluster shifts compared to the others.

The same trends are observed for the Xe–O, Xe–K, and the Xe–Xe contributions to the Xe_n cluster shieldings in the alpha cages of K*A*, shown in Table III. Furthermore, let us compare K*A* with Na*A*. For the single Xe atom in a cage, the difference in the O atom contributions provides a measure of the excluded volume effect due to the different sizes of the cations; the larger cation leads to a difference in the averaging of the chemical shift. On the other hand, the Xe-cation shielding contributions can be compared directly. We find that the K ion contributions to the average Xe shift of a single Xe atom in a cage are greater than the Na ion contributions. The net effect is a larger chemical shift for a single Xe in the cage with the larger cations. The difference between the Xe–O contributions in K*A* and Na*A* is interesting since the same $\sigma(\mathrm{Xe}\cdots\mathrm{O_{zeol}})$ and $V(\mathrm{Xe}-\mathrm{O_{zeol}})$ functions were used in the GCMC simulations in both zeolites. The smaller O contributions in K*A* arise from an excluded volume effect; the arrangements of the K ions in the cages and their larger size keep the Xe nucleus from experiencing as large O contributions to the chemical shift as it does in Na*A*. The larger contributions to the shielding from the K ions themselves make up for this, however, leading to a more deshielded Xe for a solitary Xe atom in an alpha cage of K*A* compared to Na*A*. The direct cation contribution to the chemical shift is larger for K than for Na in all cluster sizes, and this increases with cluster size. Again this appears to be more pronounced in the K*A* cage due to the in–out arrangements of the K ions. In the clusters Xe_2, Xe_3, Xe_4, and Xe_5, the observed larger incremental shifts are accounted for by somewhat larger con-

TABLE II. Calculated contributions to the Xe_n chemical shifts in a Na*A* cage, ppm at 300 K, from GCMC averaging using the shielding functions we reported in Ref. 50.

	Xe–O	Xe-cation	Xe–Xe	Total	Expt.
Xe_1	58.4	17.9	···	76.2	74.8
Xe_2	58.8	18.0	15.2	92.0	92.3
Xe_3	59.7	18.1	31.7	109.4	111.7
Xe_4	61.0	18.3	50.4	129.8	133.2
Xe_5	64.8	18.6	73.2	156.6	158.4
Xe_6	68.3	18.9	98.1	185.2	183.4
Xe_7	76.6	19.4	132.7	228.7	228.3
Xe_8	83.1	19.8	170.3	273.7	272.3

TABLE III. Calculated contributions to the Xe_n chemical shifts in a K*A* cage, ppm at 300 K, from GCMC averaging using the shielding functions we reported in Ref. 50. The differences between K*A* and Na*A* cages are also shown.

	Xe–O contrib.	Diff. K*A* − Na*A*	Xe–K contrib.	Diff. K*A* − Na*A*	Xe–Xe contrib.	Diff. K*A* − Na*A*	Total K*A*	Expt. K*A*
Xe_1	52.2	−6.2	26.5	8.6	···		78.7	79.5
Xe_2	48.6	−10.2	30.6	12.6	19.6	4.4	98.8	98.4
Xe_3	46.6	−13.1	35.0	16.9	40.8	9.1	122.4	119.7
Xe_4	46.0	−15.0	39.3	21.0	63.3	12.9	148.6	145.4
Xe_5	50.7	−14.1	45.4	26.8	96.9	23.7	192.9	180.5
Xe_6	55.7	−12.6	50.5	31.6	136.8	38.7	243.0	

tributions from the zeolite as the Xe atoms crowd against the framework with increasing size of the cluster. More important are the larger contributions from the Xe–Xe interactions. The effect of the larger excluded volume in K*A* becomes more severe as the number of Xe atoms increases due to the more pronounced deshielding exhibited by the $\sigma(r_{\mathrm{Xe-Xe}})$ function at shorter distances; thus the Xe–Xe contributions increase faster. The net effect of the larger cation size on the Xe_n clusters is therefore to increase the chemical shift, which is found experimentally, and we find this increase to be a combined effect of the larger contribution of the Xe-cation intermolecular shielding itself and the larger excluded volume from the larger cations which in turn modifies the averaging of the Xe–O and (primarily) the Xe–Xe contributions. The increments $[\delta(\mathrm{Xe}_n)-\delta(\mathrm{Xe}_{n-1})]$ increase faster in the alpha cages of zeolite K*A* than they do in Na*A*. This too is observed experimentally. Tables II and III show how well the GCMC simulations reproduce the cluster shifts in these two zeolites. Although the calculated numbers can and do change upon changing the parameters of the V(Xe–K) potential, the trends are all preserved. The differences between the chemical shift of Xe_n in K*A* and Na*A* is 4.7, 6.1, 8.0, 12.2, 22.1 ppm (observed) compared to 2.9, 6.2, 12.0, 19.0, 36.3 ppm (GCMC) for $n=1$–5. These values are in semiquantitative agreement.

Finally, the GCMC simulations reproduce the trends for the temperature dependence of the ^{129}Xe chemical shifts of the Xe_n clusters in K*A* just as well as they did for Xe_n in Na*A*.[39] The slightly more pronounced temperature dependence of the Xe_1 chemical shift in the alpha cage of K*A* compared to Xe_1 in the alpha cage of Na*A* is also reproduced by the GCMC simulations (see Fig. 6). This can be attributed to a combination of two factors: the somewhat more deshielding effect of the K^+ ion (in the zeolite) on the rare gas atom at a given r/r_0, compared to the Na^+ ion,[50] and the somewhat more attractive potential that the Xe atom finds itself in the alpha cage of K*A* compared to Na*A*. The latter is in agreement with experimental observations that the isosteric heat of each of Ar, Kr, and Xe adsorbed in K*X* is greater than that of the same rare gas in Na*X*.[48] Both factors lead to a somewhat larger ^{129}Xe chemical shift for a single Xe atom in an alpha cage of K*A* compared to an alpha cage of Na*A*. Since the same $\sigma(^{129}\mathrm{Xe}, \mathrm{Xe}\cdots\mathrm{O}_{\mathrm{zeol}})$ shielding function and $V(\mathrm{Xe}\cdots\mathrm{O}_{\mathrm{zeol}})$ potential function are used for averaging in both Na*A* and K*A* cages, the only differences between the simulations in the two cages are the different one-body distributions of the Xe in the cage (which also affects the magnitude of the average O atom contributions to the intermolecular chemical shift) and the $\sigma(^{129}\mathrm{Xe}, \mathrm{Xe}\cdots\mathrm{K}_{\mathrm{zeol}})$ shielding function being somewhat different from the $\sigma(^{129}\mathrm{Xe}, \mathrm{Xe}\cdots\mathrm{Na}_{\mathrm{zeol}})$ shielding function, thus leading to different shielding contributions to ^{129}Xe from the K^+ and Na^+ charge-balancing cations. These factors also result in the somewhat more pronounced temperature dependence of the Xe_n cluster shifts in K*A*, compared to Na*A*.

These results can be used as a basis for the interpretation of the average ^{129}Xe chemical shifts under fast exchange in various univalent cation-exchanged zeolites, where the chemical shifts are known to increase with increasing size (and polarizability) of the cation for the single Xe atom in the zeolite (that is, in the limit of zero Xe loading).[27] The physical basis and interpretation of the average ^{129}Xe chemical shift change for Xe_1 in Na*A* compared to K*A* found in this work can be applied to the ^{129}Xe chemical shift observed in the limit of zero loading in Na*Y* compared to K*Y*. Under fast exchange in these faujasites and other zeolites with open pores, the Xe atom experiences a complete averaging over a large number of cages, so that one observes a single average peak in place of the individual Xe_n cluster peaks. The observed chemical shift is then an average over the distribution of cage occupancies as well, so there is an additional factor due to the effect of the larger cation size on the detailed distributions P_n for a given overall loading. The same interpretation can be attached also to the increase in the ^{129}Xe chemical shift (at the limit of zero-loading) upon increasing fraction of exchange x in $\mathrm{Na}_{1-x}\mathrm{K}_x Y$ provided that K ion substitutes into the same positions as Na ions. Furthermore, these observations of more pronounced increases of chemical shift increments with increasing cluster size that we found for Xe_n in K*A* compared to Na*A* provide the physical basis for the interpretation of the changes in the loading dependence of the chemical shifts in cation-substituted faujasites. Without considering the changes in the *distribution* brought about by differences in cations, and assuming that the replacement cations go into the identical sites, we would predict from our results in Tables II and III an increase in the ^{129}Xe chemical shift upon K-for-Na substitution in faujasites, largely due to the excluded volume effects on the Xe–Xe contributions. This would lead to a greater increase of the average ^{129}Xe chemical shift with Xe loading upon an increase in cation size, that is, a larger slope $[d\,\delta(^{129}\mathrm{Xe})/d\langle n\rangle_{\mathrm{Xe}}]$ for the zeolite with the larger cation. In-

deed Liu *et al.* have found larger values of this slope for $K_{0.65}Na_{0.35}Y$ compared to Na*Y* in their experiments, and similar trends with Rb^+ and Cs^+ replacements.[27]

VI. CONCLUSIONS

We have observed the Xe_n clusters in the alpha cages of zeolite K*A*, their distributions, their ^{129}Xe chemical shifts, and their individual temperature dependence. The individual ^{129}Xe chemical shifts are larger than those for the corresponding Xe_n clusters in the alpha cages of zeolite Na*A*. The incremental changes in the ^{129}Xe chemical shifts with increasing cluster size are also greater for K*A* than for Na*A*. With grand canonical Monte Carlo simulations we have been able to reproduce all the observed trends in the chemical shifts. We have reproduced as well the distributions of Xe atoms among the alpha cages at equilibrium (at 573 K) which have been obtained from the intensities of individual Xe_n cluster peaks.

These results form the physical basis for the interpretation of the trends in the average ^{129}Xe chemical shifts observed under fast Xe exchange in zeolites such as Na*Y* upon univalent cation exchange, e.g., the dependence of the average ^{129}Xe chemical shift at zero xenon loading on the percentage of Na replaced in Na*Y*, and the influence of cation size on the slope of the average ^{129}Xe chemical shift with respect to xenon loading. This study of Xe_n clusters in K*A* has confirmed the direct role of size of the cation (excluded volume) in average ^{129}Xe chemical shifts in the faujasites and other open zeolites where only a single Xe peak is observed under fast exchange. One important prediction is the increase in the change of the average ^{129}Xe chemical shift with increasing $\langle n\rangle_{Xe}$, that is, *an increase in the slopes* $[d\delta(^{129}Xe)/d\langle n\rangle_{Xe}]$ *with increasing cation size*. This is a direct consequence of the larger values of the individual Xe_n cluster shifts where the larger cations leave a smaller effective volume for the Xe–Xe pairs to average over. There are, of course, changes in the distributions (fractions of cages containing *n* Xe atoms) as well, appropriate to the differences in the effective *V* (Xe-cation) potentials. But this is of secondary importance. Another important prediction is *with increasing cation size we expect an increase in the average* ^{129}Xe *chemical shift of xenon in a zeolite in the limit of zero Xe loading*. We have a direct measure of this in the value of the Xe_1 chemical shift and we find an increase in the value of $\delta(Xe_1)$ in going from Na*A* to K*A*. This is an indication that the more pronounced deshielding in the Xe-cation shielding function for larger cations, coupled with the deeper potential function for the Xe-cation effective potential, wins out over the somewhat smaller (Xe–O) contributions accompanying the increase in the r_0 of the Xe-cation potential with increasing cation size. For Xe_1 it is not the larger excluded volume from the larger cation that gives rise to a larger chemical shift as might be incorrectly concluded from an uncritical use of the ''smaller pore, larger ^{129}Xe chemical shift'' conventional wisdom;[2,13–15] rather it is the combination of the much more deshielding $\sigma(r_{\text{Xe-cation}})$ shielding function[50] combined with the deeper potential well for the larger, more polarizable ion.

ACKNOWLEDGMENT

This research has been supported by the National Science Foundation (Grant No. CHE92-10790).

[1] J. Fraissard and T. Ito, J. Chem. Phys. **76**, 5225 (1982).
[2] J. Fraissard and T. Ito, Zeolites **8**, 350 (1988).
[3] C. Dybowski, N. Bansal, and T. M. Duncan, Annu. Rev. Phys. Chem. **42**, 433 (1991).
[4] P. J. Barrie and J. Klinowski, Prog. NMR Spectrosc. **24**, 91 (1992).
[5] T. R. Stengle and K. L. Williamson, Macromolecules **20**, 1428 (1987).
[6] J. B. Miller, J. H. Walton, and C. M. Roland, Macromolecules **26**, 5602 (1993).
[7] A. P. M. Kentgens, H. A. van Boxtel, R. J. Verweel, and W. S. Veeman, Macromolecules **24**, 3712 (1991).
[8] D. J. Suh, T. J. Park, S. K. Ihm, and R. Ryoo, J. Phys. Chem. **95**, 3767 (1991).
[9] P. J. Barrie, G. F. McCann, I. Gameson, T. Rayment, and J. Klinowski, J. Phys. Chem. **95**, 9416 (1991).
[10] Q. Chen, M. A. Springel-Huet, and J. Fraissard, Chem. Phys. Lett. **159**, 117 (1989).
[11] T. T. P. Cheung, J. Phys. Chem. **93**, 7549 (1989).
[12] W. C. Conner, E. L. Weist, T. Ito, and J. Fraissard, J. Phys. Chem. **93**, 4138 (1989).
[13] E. G. Derouane and J. B. Nagy, Chem. Phys. Lett. **137**, 341 (1987).
[14] J. Demarquay and J. Fraissard, Chem. Phys. Lett. **136**, 314 (1987).
[15] D. W. Johnson and L. Griffiths, Zeolites **7**, 484 (1987).
[16] J. A. Ripmeester, C. I. Ratcliffe, and J. S. Tse, J. Chem. Soc. Faraday Trans. 1 **84**, 3731 (1988).
[17] J.-G. Kim, T. Kompany, R. Ryoo, T. Ito, and J. Fraissard, Zeolites **14**, 427 (1994).
[18] J. F. Wu, T. L. Chen, L. J. Ma, M. W. Lin, and S. B. Liu, Zeolites **12**, 86 (1992).
[19] B. F. Chmelka, J. G. Pearson, S. B. Liu, R. Ryoo, L. C. de Menorval, and A. Pines, J. Phys. Chem. **95**, 303 (1991).
[20] O. B. Yang, S. I. Woo, and R. Ryoo, J. Catal. **123**, 375 (1990).
[21] T. I. Koranyi, L. J. M. van de Ven, W. J. J. Welters, J. W. de Haan, V. H. J. de Beer, and R. A. van Santen, Catal. Lett. **17**, 105 (1993).
[22] M. Boudart, R. Ryoo, G. P. Valenca, and R. van Grieken, Catal. Lett. **17**, 273 (1993).
[23] E. Trescos, L. C. de Menorval, and F. Rachdi, J. Phys. Chem. **97**, 6943 (1993).
[24] I. C. Hwang and S. I. Woo, in *Studies in Surface Science and Catalysis, Zeolites and Related Microporous Materials: State of the Art 1994*, edited by J. Weitkamp, H. G. Kärge, H. Pfeifer, and W. Hölderich (Elsevier, Amsterdam, 1994), p. 757.
[25] H. Ihee, T. Becue, R. Ryoo, C. Potvin, J.-M. Manoli, and G. Djega-Mariadassou, in *Surface Science and Catalysis, Zeolites and Related Microporous Materials: State of the Art 1994*, edited by J. Weitkamp, H. G. Kärge, H. Pfeifer, and W. Hölderich (Elsevier, Amsterdam, 1994), p. 765.
[26] L. H. Lin and K. J. Chao, in *Surface Science and Catalysis, Zeolites and Related Microporous Materials: State of the Art 1994*, edited by J. Weitkamp, H. G. Kärge, H. Pfeifer, and W. Hölderich (Elsevier, Amsterdam, 1994), p. 749.
[27] S. B. Liu, B. M. Fung, T. C. Yang, E. C. Hong, C. T. Chang, P. C. Shih, F. H. Tong, and T. L. Chen, J. Phys. Chem. **98**, 4393 (1994).
[28] B. Boddenberg and M. Hartmann, Chem. Phys. Lett. **203**, 243 (1993).
[29] A. Gedeon, T. Ito, and J. Fraissard, Zeolites **8**, 376 (1988).
[30] J. Fraissard and J. Kärger, Zeolites **9**, 351 (1989).
[31] J. L. Bonardet, M. C. Barrage, and J. Fraissard, in *Proceedings of the 9th IZC Montreal*, edited by R. von Ballmoos *et al.* (Butterworth–Heineman, Stoneham, 1993), p. 475.
[32] M. C. Barrage, J. L. Bonardet, and J. Fraissard, Catal. Lett. **5**, 43 (1990).
[33] L. Maistriau, E. G. Derouane, and T. Ito, Zeolites **10**, 311 (1990).
[34] C. J. Jameson, A. K. Jameson, R. E. Gerald II, and A. C. de Dios, J. Chem. Phys. **96**, 1676 (1992).
[35] C. J. Jameson, A. K. Jameson, R. E. Gerald II, and A. C. de Dios, J. Chem. Phys. **96**, 1690 (1992).
[36] B. F. Chmelka, D. Raftery, A. V. McCormick, L. C. de Menorval, R. D. Levine, and A. Pines, Phys. Rev. Lett. **66**, 580 (1991); **67**, 931 (1991).
[37] A. V. McCormick and B. F. Chmelka, Mol. Phys. **73**, 603 (1991).
[38] R. G. Larsen, J. Shore, K. Schmidt-Rohr, L. Emsley, H. Long, A. Pines, M. Janicke, and B. F. Chmelka, Chem. Phys. Lett. **214**, 220 (1993).

[39] C. J. Jameson, A. K. Jameson, B. I. Baello, and H. M. Lim, J. Chem. Phys. **100**, 5965 (1994).
[40] C. J. Jameson, A. K. Jameson, H. M. Lim, and B. I. Baello, J. Chem. Phys. **100**, 5977 (1994).
[41] C. Tsiao, D. R. Corbin, and C. Dybowski, J. Phys. Chem. **94**, 867 (1990).
[42] D.-S. Shy, S.-H. Chen, J. Lievens, S. B. Liu, and K.-J. Chao, J. Chem. Soc. Faraday Trans. 1 **87**, 2855 (1991).
[43] C. J. Jameson and A. C. de Dios, J. Chem. Phys. **98**, 2208 (1993).
[44] A. K. Jameson, C. J. Jameson, A. C. de Dios, E. Oldfield, R. E. Gerald II, and G. L. Turner, Solid State NMR **4**, 1 (1995).
[45] Rex E. Gerald II, Ph.D. thesis, University of Illinois at Chicago, 1994.
[46] J. J. Pluth and J. V. Smith, J. Phys. Chem. **83**, 741 (1979).
[47] K. S. Smirnov and D. Bougeard, Zeolites **14**, 203 (1994).
[48] A. V. Kiselev and P. Q. Du, J. Chem. Soc. Faraday Trans. 2 **77**, 1 (1981).
[49] R. J.-M. Pellenq and D. Nicholson, J. Phys. Chem. **98**, 13 339 (1994).
[50] C. J. Jameson and H. M. Lim, J. Chem. Phys. **103**, 3885 (1995).
[51] M. P. Allen and D. J. Tildesley, *Computer Simulation of Liquids* (Clarendon, Oxford, 1987).
[52] G. E. Norman and V. S. Filinov, High Temp. USSR **7**, 216 (1969).
[53] J. J. Pluth and J. V. Smith, J. Am. Chem. Soc. **102**, 4704 (1980).
[54] A. K. Jameson, C. J. Jameson, and Rex Gerald II, J. Chem. Phys. **101**, 1775 (1994).
[55] A. C. de Dios (private communications).